Biogeosciences Discuss., doi:10.5194/bg-2016-195, 2016
Manuscript under review for journal Biogeosciences
Published: 9 June 2016

Biogeosciences Discussions
Open Access
EGU

Positive Indian Ocean Dipole events prevent anoxia along the west coast of India

V. Parvathi[1], I. Suresh[1], Matthieu Lengaigne[2,3], Christian Ethé[2], Jérôme Vialard[2], Marina Levy[2], S. Neetu[1], Olivier Aumont[2], Laure Resplandy[4], Hema Naik[1], Wajih Naqvi[1]

[1]CSIR-National Institute of Oceanography, Dona Paula, Goa 403 004, India
[2]LOCEAN-IPSL, Sorbonne Universités, LOCEAN (UPMC/CNRS/IRD/MNHN), Paris, France
[3] Indo-French Cell for Water Sciences, IISc-NIO-IITM–IRD Joint International Laboratory, NIO, Goa, India
[4]Scripps Institution of Oceanography, La Jolla, California, United States

Correspondence to: I. Suresh (isuresh@nio.org)

Abstract. The seasonal upwelling along the west coast of India (WCI) brings nutrient-rich, oxygen-poor subsurface waters to the continental shelf, leading to very low oxygen concentrations at shallow depths during late boreal summer and fall. This yearly-recurring coastal hypoxia is sometimes more severe, leading to coastal anoxia that has strong impacts on the living resources. In the present study, we analyze a ¼°-resolution coupled physical-biogeochemical regional oceanic simulation over the 1960-2012 period to investigate the physical processes influencing oxycline interannual variability off the WCI. Our analysis indicates a tight relationship between the oxycline and thermocline variations along the WCI at both seasonal and interannual timescales, thereby revealing a strong physical control of the WCI oxycline variability. As in observations, our model exhibits a shallow oxycline/thermocline along the WCI during fall that combines with interannual variability to create a window of opportunity for coastal anoxic events at this time of the year. We further demonstrate that boreal fall WCI oxycline fluctuations are strongly related to the Indian Ocean Dipole (IOD), with an asymmetric influence of positive and negative IOD phases. Positive IODs are associated with easterly wind anomalies near the southern tip of India. These winds force downwelling coastal Kelvin waves that propagate along the WCI and deepen the thermocline and oxycline there, thus preventing the occurrence of coastal anoxia. On the other hand, negative IOD events are associated with WCI thermocline and oxycline anomalies of opposite sign, but of smaller amplitude, and are hence a necessary, but not sufficient condition for coastal anoxia. As the IODs generally start developing in summer, these findings suggest some predictability to the occurrence of WCI coastal anoxia a couple of months ahead.

Biogeosciences Discuss., doi:10.5194/bg-2016-195, 2016
Manuscript under review for journal Biogeosciences
Published: 9 June 2016

1 Introduction

The west coast of India (WCI) is home to the largest coastal hypoxic system of the world ocean, spreading over an area of ~180,000 km^2 (Naqvi et al., 2000). These hypoxic conditions, characterized by oxygen concentration lower than 20 $\mu mol.l^{-1}$ over the entire shelf off the WCI, occur in fall, right after the southwest monsoon. Importantly, substantial year-to-year changes in both the duration and intensity of this seasonal oxygen deficiency have been reported in the literature (e.g. Naqvi et al., 2009). While the oxygen concentrations in near-bottom waters are systematically low enough to trigger conversion of oxidized nitrogen to molecular nitrogen, mostly through denitrification, in some years, this oxygen deficiency is even more severe and the bottom waters turn sulphidic, a condition called coastal anoxia (Naqvi et al., 2006). These anoxic events have tremendous impact on living resources (e.g. Diaz and Rosenberg, 2008), with more frequent episodes of fish mortality and a shorter span of fishing season, inducing decline in fish catches.

Observations from a series of ship cruises during September – October 1999 (Naqvi et al., 2000) off the WCI and time-series measurements from a fixed site off Goa since 1997 (Naqvi et al., 2009) indicate the occurrence of severe hypoxic conditions over almost the entire shelf and anoxic conditions close to the WCI, with the most intense anoxic event reported in fall 2001 and moderate ones in fall 1998 and 1999. In contrast, these data indicate that fall 1997 was characterized by far less severe hypoxic conditions. The frequent anoxic conditions occurred during the 1998-2002 period were accompanied by a three to five-fold decline in demersal fish catch in 1999 and 2001 compared to 1997. The total fish landing also remained low between 1998 and 2002, adversely affecting the economy from fisheries, and the pelagic fish catches shifted from the dominance of mackerel to oil sardine from 1998 to 1999 (Krishnakumar and Bhat, 2008). There has been a remarkable revival of fisheries since 2003, apparently due to a relaxation of the intensity of oxygen deficiency, with no severe anoxic event reported over the recent years. Subsurface oxygen concentrations have also been reported to be significantly lower for the 1997–2004 period than for the 1971–1975 period (Naqvi et al., 2009). These observations thus reveal large interannual and decadal fluctuations in the oxygen deficiency along the WCI, but the processes responsible for these variations have not yet been understood (Naqvi et al., 2009).

As opposed to other coastal hypoxic systems that have generally developed as a result of human activities (largely eutrophication) in the last few decades (Diaz and Rosenberg, 2008), the seasonal surface oxygen deficiency along the WCI is naturally driven. Indeed, the oxygen-deficient conditions that develop in early fall along the WCI result from the seasonal upwelling, which brings poorly oxygenated sub-surface waters toward the surface (Fig. 1a). The thickest Oxygen Minimum Zone (OMZ) of the world's ocean is located in this region, between 100 and 1000-m depths (e.g. Morrison et al., 1999; Naqvi, 1987; Sarma, 2002). The coastal hypoxic conditions start with the onset of the seasonal upwelling that brings these

Biogeosciences Discuss., doi:10.5194/bg-2016-195, 2016
Manuscript under review for journal Biogeosciences
Published: 9 June 2016

OMZ waters to the shelf in August and cease with end of the upwelling season in December (Banse, 1959; Carruthers et al., 1959; Pillai et al., 2000).

The main thermocline along the WCI starts to shallow in April and becomes shallowest in September-October, the peak season of the upwelling (Fig. 1a and red curve on Fig. 1b). Local winds along the WCI (black continuous curve on Fig. 1b) are favorable to upwelling only during the southwest monsoon (i.e., they have an alongshore southward component only from June to August), which indicates that the upwelling along the WCI is to a large extent forced by remote winds (Shetye et al., 1990). Alongshore wind variations in the Bay of Bengal and near the southern tip of India (STI) generate coastal Kelvin waves that propagate along the WCI at approximately 200 km.day^{-1} and influence the seasonal upwelling there (McCreary et al., 1993; Smitha et al., 2008; Shankar et al., 2002; Suresh et al., 2016). Suresh et al. (2016) further demonstrated that the wind variations in the vicinity of the STI play a major role in driving the WCI seasonal sea level and hence the upwelling. Fig.1b indeed illustrates that the westerly winds (i.e. upwelling favorable) near the STI show a better agreement with the duration of the upwelling season than the local WCI winds. The upwelling along the WCI is associated with a large-scale thermocline pattern (Fig. 1c), with coastally-trapped shallow thermocline found all along the rim of the Arabian Sea, a characteristic of coastal Kelvin waves.

Identifying the main drivers of the near-surface oxygen interannual variations in regions of the main coastal hypoxic systems is an important endeavor as it may ultimately help to predict the occurrence of severe anoxic events. The influence of large-scale climate modes on local oxygen variability has been suggested in other coastal regions. For instance, the El Niño-Southern Oscillation (ENSO) strongly influences the oxygen content along the coasts of Peru and Chile (Helly and Levine, 2004; Arntz et al., 2006; Gutierrez et al., 2008), with intensified oxygenation associated with weak El Niño upwelling and intensified hypoxia associated with strong La Niña upwelling. As in the Pacific, the natural climate variability in the Indian Ocean could be a potential candidate responsible for the near-surface oxygen interannual variations along the WCI, which has not been evaluated so far. The main indigenous mode of Indian Ocean interannual climate variability is the Indian Ocean Dipole (IOD; Saji et al., 1999; Webster et al., 1999; Murtugudde et al., 2000). A “positive” IOD is characterized by a cooling and anomalously shallow thermocline in the eastern Indian Ocean, and by a warming and anomalously deep thermocline in the central and western Indian Ocean (Fig. 1d), driven by the anomalous easterlies in the central equatorial Indian Ocean. A “negative” IOD is associated with anomalous signals of opposite polarities. The IOD usually starts developing during boreal summer and peaks in fall (e.g. Saji et al., 1999). El Niño and La Niña events tend to induce respectively the positive and negative IODs in the Indian Ocean, but IOD can also occur independent of ENSO (e.g. Annamalai et al., 2003). The IODs induce larger-amplitude, large-scale wind and thermocline-depth variations than those associated with El Niño events over the Indian Ocean (e.g. Currie et al., 2013) and thus have the potential to affect the upwelling variations along the WCI through planetary wave propagation.

Biogeosciences Discuss., doi:10.5194/bg-2016-195, 2016
Manuscript under review for journal Biogeosciences
Published: 9 June 2016

While the spatio-temporal density of observations in the eastern Pacific margin has allowed to accurately describe the monthly oxygen evolution along the west coast of South America over the past three decades (Helly and Levine, 2004; Arntz et al., 2006), there is a dearth of long-term data from fixed sites in the Indian Ocean as compared to the Pacific and the Atlantic (Gupta et al., 2016), which in turn prevents building a reliable time series that could depict the year-to-year variations. On the other hand, three-dimensional coupled physical-biogeochemical models that include the oxygen cycle have contributed to improve the description and understanding of hypoxic events dynamics in various coastal regions (Pena et al., 2010), such as the Gulf of Mexico (e.g. Hetland and DiMarco, 2008), Black Sea (e.g. Gregoire and Friedrich, 2004) and Baltic Sea (e.g. Eilola et al., 2009). Such models have also been used to describe the major mechanisms driving the spatial distribution (McCreary et al., 2013) and seasonal evolution of the OMZ in the interior of the Arabian Sea (Resplandy et al., 2012). There is, however, no dedicated modelling study to date, addressing the mechanisms that drive the interannual oxygen variability along the WCI. The present study aims at identifying the physical controls of the WCI interannual oxygen variability, with the help of a 40-year long simulation from a ¼° regional coupled physical-biogeochemical model. The horizontal resolution of our model is too coarse to resolve the dynamics on the continental shelf, but should allow identifying the large-scale processes controlling the offshore oxygen variability, which in turn control the supply of oxygen to the shelf (Gupta et al., 2016). Section 2 describes our model, the data, and the methods, and provides a brief model evaluation. Section 3 describes the main seasonal features of the thermocline and oxycline variability along the WCI in both model and observations. The strong influence of the IOD on the interannual oxycline variations along the WCI is then assessed from the model analysis in section 4. Section 5 summarizes our results and discusses them against previous studies.

2 Data and methods

2.1 Observations

We used 1°-resolution World Ocean Atlas-2013 (WOA13; Boyer et al., 2013) for evaluating the model accuracy at representing the large-scale climatological temperature and oxygen. The sea level being a good proxy for vertical movements of the thermocline in tropical regions (e.g. Fukumori et al., 1998), we used the sea-level data from satellite altimetry produced by Ssalto/Duacs and distributed by AVISO (http://www.aviso.altimetry.fr/duacs/) as a proxy for the thermocline interannual variability along the WCI. In addition, we used the monthly level 3 Ocean Color Climate Change Initiative (OC-CCI) product, available at http://www.oceancolour.org/, that merges data from the SeaWiFs, MERIS and MODIS ocean color missions to evaluate the model surface chlorophyll climatological seasonal cycle.

We also used the measurements from Candolim Time Series (CaTS) station located along the WCI in the inner shelf off Goa (~15.5°N; 73.6°E) to construct a seasonal cycle of oxygen variations near the coast. This station has been established by CSIR-National Institute of Oceanography (CSIR-NIO) and records the physical (temperature, salinity) and biogeochemical (oxygen, nitrate, nitrite, hydrogen sulphide, etc.) parameters from September 1997 onwards (see Maya et al., 2011 for a

Biogeosciences Discuss., doi:10.5194/bg-2016-195, 2016
Manuscript under review for journal Biogeosciences
Published: 9 June 2016

detailed description). This site lies approximately 10 km off the Candolim beach, where the depth of the water column is ~28m. Samples are taken at four depths: just below the surface, just above the bottom, and at two intermediate depths equally spaced between the surface and bottom. This dataset consists of a total of 142 vertical profiles during the 1997-2010 period and has been extensively used by the previous studies (e.g., Naqvi et al., 2006, 2009, 2010a). Fig. 2a shows the percentage of years sampled month-wise in this dataset. It indicates that in-situ measurements have been performed at this station ~50% of the years over the 1997-2010 period for most calendar months, including September-October (the time of peaking of anoxic events), except for June (< 10%) and July (no data), when summer monsoon rough weather conditions prevent observations (Naqvi et al., 2009). This temporal coverage allows us to build a reliable monthly climatology of near-coastal oxygen variations, except for the month of June and July. Though CaTS offers the best available dataset to study the oxygen variations along the WCI, a thorough description of oxygen interannual variability is limited by two reasons. First, during our period of interest, i.e., September – October, the temporal distribution of the data indicates only ~50% of the years were sampled over the 1997-2010 period. Second, the months for which a large number of records are available reveal very different vertical oxygen profile over the same month (like in September 1998 or 2000; Figs. 2cand 2e), highlighting the existence of a large variability at sub-monthly timescale. For some other months, the number of available profiles is very limited, like in September 1999, when only one profile is available (Fig. 2d). Given the existing high frequency variability, averaging this very limited number of profiles may not provide a value, representative of the actual monthly average. As a result, the uneven temporal distribution and the sub-monthly variability do not allow us to build a reliable monthly pluri-annual time series from this dataset. We will hence identify the years when severe oxygen deficiency occurs from Table 1 of Naqvi et al. (2009), which is based on the absence of nitrate and nitrite and the presence of hydrogen sulphide in the water column. These years are marked as black stars on Fig. 11b and will be further discussed at the end of this paper.

2.2 Model description

The model used in this study couples the NEMO (Nucleus for European Modelling of the Ocean; Madec, 2008) physical ocean component with the PISCES (Pelagic Interaction Scheme for Carbon and Ecosystem Studies; Aumont et al., 2015) biogeochemical component through the OASIS3 (Valcke, 2013) coupler. The PISCES model has 24 compartments, which include two sizes of sinking particles and four "living" biological pools, representing two phytoplankton (nano-phytoplankton and diatoms) and two zooplankton (microzooplankton and meso-zooplankton) size classes. Phytoplankton growth is limited by five nutrients: NO3, NH4, PO4, SiO4, and Fe. The ratios among C, N, and P are kept constant for the "living" compartments, at values proposed by Takahashi et al. (1985). The internal Fe contents of both phytoplankton groups and Si contents of diatoms are prognostically simulated as a function of ambient concentrations in nutrients and light level. Details on the red-green-blue model from which light penetration profiles are calculated are given in Lengaigne et al. (2007). The Chl/C ratio is modelled using a modified version of the photo-adaptation model by Geider et al. (1998). Dissolved

Biogeosciences Discuss., doi:10.5194/bg-2016-195, 2016
Manuscript under review for journal Biogeosciences
Published: 9 June 2016

oxygen is prognostic and evolves in response to physical conditions (advection, mixing), biological sources and sinks and the air-sea fluxes:

$$\partial_t O_2 = \underbrace{\left(\frac{\partial O_2}{\partial t}\right)_{Dyn}}_{Dynamical\ transport} + \underbrace{\left(\frac{\partial O_2}{\partial t}\right)_{Bio}}_{Biological\ sources\ and\ sinks} + J_{flux}$$

where$(\partial O_2/\partial t)_{Bio}$includes all biological processes affecting the concentration of O_2, $(\partial O_2/\partial t)_{Dyn}$accounts for large scale and turbulent transport of oxygen and J_{flux} is the contribution of O_2 air–sea fluxes.

The response of oxygen to biological processes $(\partial O_2/\partial t)_{Bio}$is computed as follows:

$$\left(\frac{\partial O_2}{\partial t}\right)_{Bio} = \underbrace{(R^1_{o:c} + R^2_{o:c})\left(\mu^P_{NO_3} P + \mu^D_{NO_3} D\right)}_{New\ Production}$$
$$\underbrace{+R^1_{o:c}\left(\mu^P_{NH_4} P + \mu^D_{NH_4} D\right)}_{Regenerated\ Production} - \underbrace{\lambda^*_{DOC} f(O_2) DOC}_{Reminralization}$$
$$\underbrace{-G^Z Z - G^M M}_{Respiration} - \underbrace{R^2_{o:c} Nitrif}_{Nitrification}$$

Oxygen is produced during photosynthesis (calculating the uptake of nitrate and ammonium by phytoplankton separately) by nanophytoplankton (P) and diatoms (D) and consumed by dissolved organic matter (DOC) remineralization, small (Z) and large (M) zooplankton respiration, and nitrification. This last term represents the conversion of ammonium into nitrate and is assumed to be photo-inhibited and reduced in suboxic waters. It is therefore a function of the ammonium and oxygen concentrations and photosynthetically available radiation.

The response of oxygen to dynamical processes is computed as:

$$\left(\frac{\partial O_2}{\partial t}\right)_{Dyn} = \underbrace{-u_H \cdot \nabla_H O_2}_{lateral\ advection} - \underbrace{w \cdot \nabla_H O_2}_{vertical\ advection} + \underbrace{\frac{\partial K_z \partial O_2}{\partial z^2}}_{vertical\ mixing}$$

where u_H and w are respectively the horizontal and vertical currents and $K_z$is the vertical mixing coefficient.

Finally, J_{flux} is the flux of O2 from air to sea (F_{O_2}) divided by the depth of model surface layer, where

$$F_{O_2} = k_w(\alpha O_{2atm} - O_2)$$

Biogeosciences Discuss., doi:10.5194/bg-2016-195, 2016
Manuscript under review for journal Biogeosciences
Published: 9 June 2016

k_w is the transfer velocity, $(\alpha O_{2atm} - O_2)$ is the difference in O_2 partial pressure between the air and surface sea water, and α the solubility of O_2 in seawater.

For a more detailed description, manuals for NEMO and PISCES are available online at http://www.nemo-ocean.eu/About-NEMO/Reference-manuals. This coupled model has been successfully applied to various studies in the Indian Ocean (e.g. Kone et al., 2009; Resplandy et al. 2009; Currie et al., 2013), including the Arabian Sea OMZ (Resplandy et al., 2011, 2012).

The regional configuration used in the following is an Indian Ocean sub-domain from the global ¼° resolution (i.e. cell size ~25 km) configuration described by Barnier et al. (2006). It has 46 vertical levels, with a resolution ranging from 5m at the surface to 250m at the bottom. The African continent closes the western boundary of the domain. The oceanic portions of the eastern, northern and southern boundaries use radiative open boundaries (Treguier et al., 2001), constrained with a 150-day timescale relaxation to physical and biogeochemical inputs from a global simulation (Dussin et al., 2009). The circulation and thermodynamics of this regional configuration have been extensively evaluated and shown to reproduce observed intraseasonal variations of key physical parameters well in several Indian Ocean regions (Praveen Kumar et al., 2014), including the Arabian Sea (Nisha et al., 2013; Vialard et al., 2013; Keerthi et al., 2015) and the Bay of Bengal (Akhil et al., 2014, 2016).

The simulation starts from rest and the temperature and salinity are initialized from the WOA13 climatology (Boyer et al., 2013). PISCES biogeochemical tracers are initialized from the WOA13 database for nutrients and global simulation climatology for other tracers (Aumont and Bopp, 2006). After 5 years of spin-up with climatological surface and lateral boundary forcing, the model is forced with the Drakkar Forcing Set #4.4 (DFS4.4, Brodeau et al., 2009) from 1958 to 2012. This forcing is a modified version of the CORE dataset (Large and Yeager, 2004), with atmospheric parameters derived from ERA40 reanalysis until 2002 (Uppala et al., 2005) and ECMWF analysis after 2002 for latent and sensible heat fluxes computation. Radiative fluxes are taken from the corrected International Satellite Cloud Climatology Project-Flux Dataset (ISCCP-FD) surface radiations (Zhang et al., 2004) while precipitation are specified from a blend of satellite products described in Large and Yeager (2004). All atmospheric fields are corrected to avoid temporal discontinuities and to remove known biases (see Brodeau et al., 2009 for details). In the following, the 1960-2012 period is analysed.

2.3 Model climatology

The model's ability to capture the climatological surface chlorophyll concentrations during the summer and winter monsoons is shown in Fig. 3. During the summer monsoon (Fig. 3a), seasonal blooms are observed along the coasts of the Arabian Peninsula and along the WCI in response to coastal upwelling that brings nutrients into the euphotic layer (e.g. Wiggert et al., 2005; Levy et al., 2007; Koné et al., 2009). The chlorophyll signal along the Somalia and Omani coasts extends offshore towards the central Arabian Sea (Fig. 3a) through offshore lateral advection of nutrients from upwelling

Biogeosciences Discuss., doi:10.5194/bg-2016-195, 2016
Manuscript under review for journal Biogeosciences
Published: 9 June 2016

regions, either by large-scale circulation or by eddy activity (e.g. Lee et al., 2000; Resplandy et al., 2011). During the winter monsoon(Fig. 3b), the cool, dry northeasterly winds in the Arabian Sea induce convective mixing and entrain nutrient-rich waters to the surface, triggering the chlorophyll bloom observed north of 15°N (Madhupratap et al., 1996). The model generally accurately reproduces these seasonal chlorophyll patterns (Figs. 3c and 3d). As for observations, the largest chlorophyll bloom in summer occurs in the western Arabian Sea, with strong signals along the rim of the Northern Indian Ocean, while winter is characterized by oligotrophic conditions in the southeastern Arabian Sea and higher concentrations in the northern and western parts. The largest discrepancy between modelled and satellite chlorophyll is an overall overestimation of the amplitude of the summer blooms, in the western Arabian Sea, east of Sri Lanka and around the rim the Bay of Bengal (Figs. 3a and 3c).

The comparison of the modelled horizontal and vertical climatological oxygen distribution with that of WOA13 is further shown in Fig. 4. In observations, the core of the OMZ is confined to the northern part of the basin (Fig. 4a) and expands vertically between 150 and 1000-m depth (Fig. 4b), and the lowest subsurface oxygen concentrations are found in the central/eastern part of the basin. The OMZ is thus shifted to the east of the region of highest biological production located along the west coast of the Arabian Sea (Fig. 3). The oxycline lies around ~100m, and is slightly shallower on the western and eastern part of the basin (Fig. 4b), because of the seasonal upwelling systems there. The model captures these observed oxygen patterns, with poorly-oxygenated water confined to the northern Arabian Sea and high-oxygenated water found near the equator and farther south, and an OMZ core located in the eastern part of the Arabian Sea despite a slight overestimation of the modelled oxygen content at depth in the Arabian Sea (Fig. 4b vs Fig. 4d). We can also note that the model underestimates the depth of the OMZ core (~200m in the model and ~300m in observations). The upper ocean vertical oxygen distribution is also well captured, with a model oxycline depth around 100m (Fig. 4d), similar to the observed one (Fig. 4c).

2.4 Thermocline and oxycline depths

Both temperature and dissolved oxygen decrease with increasing depth below the mixed layer (Figs. 4b and d). The oxycline or thermocline depths are usually defined as the depths of maximum gradient. It is however customary to approximate those depths from a fixed isocontour, especially in tropical regions. Resplandy et al. (2012) used the depth of 100 $\mu mol.l^{-1}$ as a proxy for the oxycline depth in their study, whereas Prakash et al. (2013) used 50 $\mu mol.l^{-1}$. Here, we define the oxycline depth (hereafter OCD) as the depth of the 100 $\mu mol.l^{-1}$ oxygen isocontour (following Resplandy et al., 2012) and the thermocline depth (hereafter TCD) as the depth of 23^{o} C isotherm (following Prakash et al., 2013). The conclusions of our study are not sensitive to the above choices, i.e., the results discussed below are similar when considering the 50 $\mu mol.l^{-1}$ or 150 $\mu mol.l^{-1}$ instead of 100 $\mu mol.l^{-1}$, to define the oxycline depth and 20°C or 25°C instead of 23°C to define the thermocline depth. The OCD and TCD were both derived from observed or modelled profiles using linear interpolation.

Biogeosciences Discuss., doi:10.5194/bg-2016-195, 2016
Manuscript under review for journal Biogeosciences
Published: 9 June 2016

2.5 IOD index

To characterize the IOD variability, we used the standard Dipole Mode Index (DMI, Saji et al., 1999), which is calculated as the difference between the interannual SST anomalies in the western (50°E-70°E; 10°N-10°S) and southeastern (90°E-110°E; 10°S-0°) equatorial Indian Ocean in September–November. For consistency, we used the DMI derived from the model SST, but the very high correlation between the DMI based on model and observations (~0.87) make our results fairly insensitive to the choice of either of them. This index has been normalized by its standard deviation to make it dimensionless. Interannual anomalies are calculated from monthly time-series by subtracting the 1960-2012 mean seasonal cycle and applying a 3-month smoothing to remove sub-seasonal variations.

3 Results

3.1 Dynamical control of the oxycline variability along the WCI

The seasonality of the oxygen concentration within the OMZ is very weak, but this is not the case for the OCD (Resplandy et al., 2012). Fig. 1a suggests a strong link between the seasonal variations of the OCD and TCD along the WCI. The strong correlation between the thermocline and oxycline has already been observed in many regions (e.g., Morales et al., 1999; Prakash et al., 2013). This is expected in regions, where the effects of biological processes and of vertical mixing are small in comparison to those of vertical advection, which is generally the case at the thermocline depth. In such regions, vertical oceanic velocities act in the same way on the oxygen and temperature isolines, lifting or lowering them in phase. Figs. 5a and 5b quantify this relationship by displaying the correlation between the seasonal OCD and TCD variations in the Northern Indian Ocean. For both observations and model, this correlation exceeds 0.7 everywhere in the Arabian Sea, except in a small region off the Horn of Africa, possibly because of strong lateral advection there. These correlations drop in the equatorial region, presumably because our oxycline definition (100 $\mu mol.l^{-1}$) corresponds to a lower temperature criterion than 23°C in these regions. The model in general exhibits higher OCD-TCD correlations than for observations, especially in the eastern Bay of Bengal where observed OCD and TCD are not well correlated. The tight OCD-TCD relationship along the WCI implies a strong control of oxygen variability by the upwelling intensity in our region of interest.

The tight relation between the OCD and TCD in the eastern Arabian Sea is further illustrated in Fig. 6, which displays the observed and modelled OCD and TCD seasonal climatologies. During the spring inter monsoon (March-May), the TCD and OCD are spatially quite uniform and deep (~100m) in the eastern Arabian Sea (Figs. 6a and 6e). The shallow OCD/TCD near the STI during this season indicates that the wind is already favorable to upwelling there (Figs. 6a and 6e and dashed curve on Fig. 1b). With the advent of the summer monsoon (June-August), the westerly monsoon winds drive a very strong offshore Ekman transport in the western Bay of Bengal and near the STI (Suresh et al., 2016), resulting in an upwelling signal, which shoals the OCD/TCD up to 60m at the STI (Figs. 6b and 6f; Smitha et al., 2008; Gupta et al., 2016). Further north, the winds are almost perpendicular to the coast of western India (Suresh et al., 2016) and hence do not directly induce

Biogeosciences Discuss., doi:10.5194/bg-2016-195, 2016
Manuscript under review for journal Biogeosciences
Published: 9 June 2016

upwelling there. The shallow OCD/TCD signal from the STI propagates northward along the western Indian coast as an upwelling coastal Kelvin wave (Figs. 6b and 6f). By the end of the southwest monsoon (September-October-November), shallow OCD/TCD can be seen along the entire Arabian Sea coastal rim, largely as the result of the remotely-forced coastal Kelvin waves. From December to February, winds at the STI and alongshore winds further north are both favorable to downwelling (Figs. 6d, 6h and 1b), thus leading to deepening of the TCD and OCD along the WCI (Figs. 6d and 6h). Part of the strong downwelling signal at the coast during the preceding season (Figs. 6c and 6g) is radiated westward as a planetary wave (e.g. McCreary et al., 1993, Suresh et al., 2016). This is clearly shown in the model, where the shape of the deep OCD/TCD pattern is clearly suggestive of faster planetary wave propagation at lower latitudes (Fig. 6h). The striking similarity in the seasonal patterns of OCD and TCD again indicates a strong physical control of the eastern Arabian Sea OCD at the seasonal timescale. This echoes results of Resplandy et al. (2012), who found that upper-ocean oxygen seasonality primarily arises from vertical movements at the thermocline level forced by both local and remote wind forcing.

The observed and modelled seasonal oxycline climatologies along the WCI (box shown in Figs. 1c and 5) are further illustrated in Fig. 7. The modelled and observed climatologies match very well for the entire year, a pre-requisite for using the model for understanding the processes of interannual oxycline variability there. Consistent with previous figures, the oxycline starts shoaling at the beginning of the summer monsoon (April-May), becomes shallowest by September-October and then starts deepening again by November. In addition to this seasonal evolution, Fig. 7 also provides an estimation of the amplitude of the interannual OCD variability at WCI from the model. The amplitude of OCD interannual variability is comparatively larger by the end of the year, i.e., during September - December. A seasonally shallow OCD combined with a larger interannual variability in fall creates a window of opportunity for coastal anoxic events to occur during September-November (hereafter SON). This is consistent with previous observations of oxygen deficiency along the WCI (e.g., Naqvi et al., 2000, 2009; Gupta et al., 2016).

The previous comparison focuses on open-ocean variability. In order to verify that this variability is representative of anoxic conditions that occur on the shelf, we now compare the climatological near-surface oxygen contents (0-40m average) obtained from the model and WOA13 in the WCI box with those obtained from the CaTS on the shelf (Fig. 8a). Despite lower oxygen content on the shelf, there is a very good phase agreement of seasonal variations between shelf data and the two offshore datasets. The lower oxygen content along the shelf is expected because of the coastal upwelling resulting in shoaling of the oxycline, and also because of the local consumption of oxygen. The good phase agreement is also indicative of the strong connection between the coastal and offshore oxygen variability through dynamical upwelling processes. Figs. 8b and 8c show the monthly percentages of occurrence of hypoxic profiles from CaTS (on the shelf) data and the model (offshore). Since the upper oxygen content and vertical profile are different at the coast and offshore, we have used different thresholds to detect hypoxic profiles in the observation and the model. Consistent with previous literature, anoxic events are most likely to occur from August to November in the model and the shelf data, as expected from the very shallow

Biogeosciences Discuss., doi:10.5194/bg-2016-195, 2016
Manuscript under review for journal Biogeosciences
Published: 9 June 2016

background oxycline at that time of the year. This justifies our focus on the fall period for analyzing the processes that drive the modelled interannual variability of the WCI oxycline in the following.

We previously demonstrated a tight connection between the variability of the OCD and the TCD in the eastern Arabian Sea at the seasonal timescale. Fig. 9a exhibits a similar relation for fall modelled interannual OCD and TCD anomalies. A comparison with observations is unfortunately not feasible due to lack of a basin-scale dataset for interannual oxycline anomalies. The model predicts poorer OCD-TCD correlations at interannual than at the seasonal timescale in the upwelling regions of western Arabian Sea (Fig. 9a). Interannual OCD and TCD correlations are, in general, slightly weaker than at seasonal timescales, but remain high in a large part of the Indian Ocean north of 5°N, generally exceeding 0.8 in the entire Bay of Bengal and in the eastern Arabian Sea, and in particular in the WCI box (~0.89 correlation). Due to the unavailability of continuous oxygen observations in the WCI region (see Section 2.1), we cannot directly evaluate the modelled oxygen interannual variability there. We however evaluate the modelled TCD interannual variability, which is closely tied to the OCD interannual variability. The modeled interannual TCD anomalies in the WCI box (red curve on Fig. 9b) agree well (0.86 correlation) with sea-level interannual anomalies from altimeter measurements (blue curve on Fig. 9b, a good proxy of thermocline depth variations in stratified regions). Model TCD and observed sea level indicate strongest thermocline shoaling in fall 1999 and deeper than usual thermocline in fall 1994, 1997 and 2008. We use the model ability to capture observed thermocline depth interannual variations along the WCI to further examine the processes responsible for the OCD interannual variability there.

3.2 The IOD control on the oxycline interannual variability along the WCI

The relationships between the modeled interannual variability of the OCD along the WCI and that of the OCD, TCD, SST and wind at the basin scale are demonstrated in Figs. 10a-c, which show regression maps of interannual anomalies of these variables to the time series of the fall OCD anomalies in the WCI box. The fall WCI OCD variations are not merely local, but are associated with basin-scale ocean-atmosphere interannual fluctuations over the entire equatorial and northern Indian Ocean. An anomalously deep OCD along the WCI is usually associated with deeper OCD and TCD in the southeastern Arabian Sea and in the vicinity of Sri Lanka and the STI (Fig. 10a,b). Positive OCD anomalies along the WCI are also related to shallower OCD and TCD in the eastern Indian Ocean and along the eastern rim of the Bay of Bengal. The associated large-scale wind patterns (Fig. 10c) explain these interannual OCD and TCD patterns. Anomalous easterlies at the equator force an equatorial upwelling Kelvin wave that shoals the OCD and TCD in the eastern equatorial Indian Ocean. This equatorial Kelvin wave further propagates around the rim of the Bay as a coastal upwelling Kelvin wave, thereby shoaling the TCD and OCD there. Similar to what happens at the seasonal scale, zonal wind stress anomalies in the vicinity of Sri Lanka and the STI force a downwelling coastal Kelvin wave that propagates poleward along the western Indian coastline, resulting in a deepening of the TCD and OCD there. The strong correlation between the interannual fluctuations in OCD along the WCI and those in zonal winds at the STI (up to 0.65; see color shading on Fig. 10c) further illustrates the

Biogeosciences Discuss., doi:10.5194/bg-2016-195, 2016
Manuscript under review for journal Biogeosciences
Published: 9 June 2016

strong influence of these winds in driving OCD and TCD interannual fluctuations in the southeastern part of the Arabian Sea. As shown in Fig. 10b, these variations are also related to anomalous SST patterns characterized by a strong cooling south of the equator in the eastern Indian Ocean and a weaker warming in the western portion of the basin.

The TCD, SST and wind patterns shown on Fig. 10b,c are reminiscent of the IOD signature (Fig. 1d), an Indian-Ocean coupled ocean-atmosphere climate mode that peaks in fall, as discussed in the introduction. This is further demonstrated in Fig. 10d-f, which displays regression maps of interannual anomalies of OCD, TCD, SST, and winds onto the boreal fall DMI. The resulting patterns, representing the typical response to a positive IOD phase, are very similar to those displayed in Fig. 10a-c. These similar patterns highlight the strong link between IOD events and WCI oxycline year-to-year variations. We further examine the relationship between the WCI OCD and the IOD in Fig. 11a, which displays timeseries of fall OCD interannual anomalies and the fall DMI. Consistent with the regression map, we find a high correlation (~0.67) between the DMI and OCD along the WCI. However, the influences of positive and negative phases of IOD on the WCI OCD (and TCD, not shown) are not symmetrical (Fig. 11a): most of the positive IOD events cause a deepening of OCD along WCI (e.g., 1961, 1967, 1994, 1997), while negative IOD can either be associated with a shoaling (e.g. 1996, 1998, 2010) or a deepening (e.g. 1979-81). To further illustrate this asymmetry, Fig. 11b provides a scatterplot of the fall DMI versus the fall interannual anomalies of OCD along the WCI. This scatterplot confirms that there is an asymmetric impact of positive/negative IODs on the OCD along the WCI. The WCI OCD response to positive IODs is very robust, with positive IOD events (DMI > 1°C) being systematically associated with a deepening, with a regression slope of 5-m deepening per °C DMI for positive DMI values. The WCI response to negative IOD is weaker and much less systematic. As already discussed from Fig. 11a, negative IOD events (DMI<-1°C) are generally related to negative OCD anomalies but can also be related to positive OCD anomalies. The regression slope for negative DMI values is not significantly different from zero at the 95% confidence level (Fig. 11b). Fig. 12 finally provides a composite of the temporal evolution of the anomalous OCD and TCD along the WCI along with zonal wind stress variations at the STI for signal associated with positive/negative IOD events. Fig. 12a,b illustrates again the two to three times weaker response of the WCI OCD for negative compared to positive IOD events. This weaker response is related to weaker zonal wind anomalies at the STI (Fig. 12c) that consequently trigger a weaker coastal Kelvin wave response and thus weaker WCI TCD/OCD anomalies. It is therefore likely that the weaker and less robust wind signal associated with negative IODs at the STI compared to positive IODs may explain part of the asymmetry seen in Fig. 11.

4 Summary and Discussion

4.1 Summary

The year-to-year variations of coastal hypoxia along the WCI have been identified fifteen years ago, along with their strong impacts on fisheries and ecosystem. The mechanisms controlling these variations have however not yet been elucidated. The

Biogeosciences Discuss., doi:10.5194/bg-2016-195, 2016
Manuscript under review for journal Biogeosciences
Published: 9 June 2016

present study offers new insights on the physical controls of coastal hypoxia along the WCI. To that end, we used an eddy-permitting (¼°horizontal resolution), regional Indian Ocean configuration of a coupled physical-biogeochemical model. The simulation spans a period long enough (1960-2012) to allow analyzing the driving mechanisms of oxygen interannual variability along the WCI. The model accurately reproduces the oxycline and thermocline seasonal cycle off the WCI, with a seasonal upwelling that yields shallowest oxycline/thermocline at the end of the summer monsoon. The modelled and observed offshore climatological seasonal cycles match in-situ measurements on the shelf, with a strongest seasonal oxygen deficiency and occurrence rate of anoxic events during boreal fall. It is suggested that the upwelling of oxygen-depleted subsurface waters at the shelf break mainly causes the anoxic events over the western Indian continental shelf.

The shallow oxycline in fall combines with a large interannual variability at this time of the year to create a window of opportunity for coastal anoxic events. Our model analysis further indicates that there is a tight coupling between the thermocline and oxycline variability in this region at both seasonal and interannual timescales, indicative of a strong physical control of the oxygen variability through vertical advection. Interannual thermocline fluctuations along the WCI are related to basin-scale wind, thermocline and oxycline depth perturbations associated with Indian Ocean Dipole (IOD) events, an Indian Ocean coupled ocean-atmosphere climate mode that peaks in fall. Positive IOD events are associated with easterly wind anomalies in the central equatorial Indian Ocean, which extend meridionally up to the STI. These easterly wind anomalies trigger downwelling coastal Kelvin waves that propagate along the WCI and deepen the thermocline and oxycline in boreal fall, thereby preventing the occurrence of coastal anoxia off the WCI during positive IOD events. Our model results also suggest an asymmetry between the impact of positive and negative IOD events on the WCI oxycline depth. The westerly wind anomalies at the STI indeed have a smaller amplitude during negative IODs than their easterly counterparts during positive IODs, thus resulting in a weaker and less consistent shoaling of OCD along WCI during negative IOD events.

4.2 Discussion

Previous studies have demonstrated the impact of large-scale climate modes on year-to-year variations of the oxygen deficiencies in coastal hypoxic systems. In the Pacific, El Niño conditions lead to intensified oxygenation along the coasts of Peru and Chile as a result of weak upwelling (e.g., Arntz et al., 2006; Gutierrez et al., 2008), while in the Atlantic, the Benguela Niño leads to intensified anoxia along the Namibian shelf (Monteiro et al., 2008). The western continental shelf of India is home to the largest naturally-formed coastal hypoxic system in the world. In this study, we identify for the first time the IOD as a major climatic driver of the year-to-year oxycline and thermocline variations along the WCI. Though the IOD has a weaker thermocline depth signature on the west than on the east coast of India, it has stronger societal consequences as it influences the WCI seasonal upwelling that brings suboxic waters very close to the surface during fall. The IOD influence is further shown to be larger for positive than negative IOD events. Although the IOD influence on the west Indian coast has never been reported so far, it has regularly been reported in the in the Bay of Bengal. In line with our results, Aparna et al.

Biogeosciences Discuss., doi:10.5194/bg-2016-195, 2016
Manuscript under review for journal Biogeosciences
Published: 9 June 2016

(2012) indeed showed that IOD events drive strong sea-level and thermocline fluctuations along the rim of the Bay in fall, through coastal Kelvin wave propagation from the equatorial region. Akhil et al. (2016) further demonstrated that this remote forcing also drives anti-clockwise anomalous horizontal currents in fall in the Bay, which in turn leads to large interannual variations of Sea Surface Salinity in the southern Andaman Sea. On the biogeochemical side, Wiggert et al. (2002, 2009) and Currie et al. (2013) demonstrated that IOD events are responsible for large interannual chlorophyll variations in the southeastern Bay of Bengal and at the STI. Finally, the asymmetrical IOD signature found in Arabian Sea in the present study has already been described for the Bay of Bengal in terms of sea-level (Aparna et al., 2012) and chlorophyll (Currie et al., 2013). Although our results suggest that part of this asymmetry may be explained by the difference in the strength of winds at STI associated with each phase of the IOD, an in-depth investigation of the processes that control the thermocline along the WCI in response to positive and negative IOD events is required.

Our findings partly explain the substantial year-to-year changes in both the duration and intensity of the observed seasonal oxygen deficiency over the western Indian shelf (Naqvi et al., 2009). None of the anoxic events reported by Naqvi et al. (2009) (black stars in Fig. 11b) lies on the upper right quadrant of the scatterplot shown in Fig. 11b, indicating that positive IODs systematically prevent the occurrence of anoxic events. For instance, the relaxation of anoxic condition in early fall 1997 reported by Naqvi et al. (2009) is in line with the occurrence of very strong positive IOD during that year. Most anoxic events are found in the lower left quadrant, i.e., near neutral or negative IOD conditions and anomalously shallow offshore oxycline. Neutral or negative IOD years are however not necessarily anoxic, indicating that a neutral or negative IOD is a necessary but not a sufficient condition for severe anoxia. A recent study by Gupta et al. (2016) revealed that the oxygen deficiency in 1959 along the WCI was more severe than in 2012, a conclusion consistent with the occurrence of a negative IOD in 1959 and a positive one in 2012. Similarly, in-situ measurements also revealed that subsurface oxygen concentrations were significantly lower at the turn of the 20th century than in the 70's (Naqvi et al., 2009): our simulation exhibit a similar behavior (see Fig. 11a), showing many years with shallower than normal OCD in the later period and systematically deeper than normal OCD during 1970's. The causes for those decadal variations need to be investigated in greater detail.

The ~0.7 correlation between IOD variability and oxycline variations along the WCI implies that ~50% of the interannual oxycline variance is explained by the IOD at this location. This relationship between the IOD and year-to-year variations of seasonal anoxic conditions along the shelf may facilitate advance warning for the possible occurrence of severe anoxic events. Recent studies indeed indicate that skillful predictions of mature IOD events in fall can be achieved about one season ahead (e.g. Luo et al., 2007; Wang et al., 2009; Zhao and Hendon 2009; Sooraj et al., 2012) and up to two seasons ahead in the case of large IOD events (Luo et al., 2007, 2008; Shi et al., 2012). Those predictions of IOD events should allow providing a warning about the likelihood of severe anoxic conditions along the WCI during spring or summer. A predicted positive IOD is indeed associated with very low chances of such an anoxic event, while neutral or negative IOD conditions may be associated with the occurrence of such an event.

Biogeosciences Discuss., doi:10.5194/bg-2016-195, 2016
Manuscript under review for journal Biogeosciences
Published: 9 June 2016

It must however be kept in mind that other factors are also likely to contribute to the reported interannual fluctuations of hypoxic conditions in this region. Naqvi et al. (2009) for instance suggested that increased productivity due to increased nutrient loading from land associated with anthropogenic activities might have the potential to trigger a shift from natural suboxic to anthropogenic anoxic conditions during recent decades. This hypothesis however cannot explain the relaxation of the intensity of oxygen deficiency in the recent decades. Another contributing factor could be related with changes in local hydrographic variations. For instance, interannual variations of the land runoff along the Western Ghats, local precipitation during summer monsoon or input of Bay of Bengal freshwater during the northeast monsoon (e.g. Jensen et al., 2001) could modulate the upper ocean haline stratification, ventilation of the subsurface waters and hence the subsurface oxygen content along the WCI. Finally, local alongshore wind variations may modulate the intensity of coastal upwelling and hence the amount of oxygen-depleted waters brought to the shelf. The influence of these factors hence requires further investigation.

The present study has some inherent limitations though. The horizontal resolution of the model (1/4°) does not resolve the fine-scale interactions between the shelf and the deep ocean, including the detailed structure of the coastal upwelling. Our model is eddy-permitting, but not really eddy-resolving, and hence does not capture oceanic mesoscale eddies, which play an important role for coastal-offshore exchanges. Increasing the upper-ocean vertical resolution and accounting for WCI runoffs interannual variability (which are climatological in the present setup) may also improve the representation of the upper-ocean stratification, subsurface ventilation and oxygen variability along the WCI. On the observational front, the current spatio-temporal sampling does not allow building reliable long-term time series of the month-to-month oxygen variations along the shelf and offshore. Despite the establishment of frequent measurements of oxygen profile off Goa since September 1997, the numerous unsampled months (July and August are almost unsampled because of rough weather conditions) and the strong sub-monthly variability prevent a continuous monitoring of oxygen variations along the WCI. A reasonable number of moorings or Argo drifters with oxygen and temperature sensors along the shelf and further offshore would allow a finer description of the oxygen variability, its relationship with temperature and connection with the offshore variations.

Though the present study is focused on the WCI, our Indian Ocean configuration model allows assessing other regions where near-surface hypoxia can occur. Fig.13 shows the percentage of profiles where oxygen concentrations below 80 $\mu mol.l^{-1}$ occur within the top 50 m. This threshold is indicative of the limit under which many organisms start to suffer from physiological stress that could ultimately lead to death (Vaquer-Sunyer and Duarte, 2008). This analysis indicates that the coast of Oman can also experience hypoxic conditions as reported in the literature (e.g., Piontovski and Al-Oufi, 2015), although hypoxia along Oman is never as severe as along the WCI (Naqvi et al., 2010b). Fig. 13 indicates that the northwestern Bay of Bengal can also experience near-surface low-level oxygen concentrations, as reported from a series of ship cruise measurements by Sarma et al. (2013). Further examination of the mechanisms driving these hypoxic events reveal that the IOD strongly impacts the oxygen variability in the northwestern Bay of Bengal: positive IOD events generally inducing a shoaling of the oxycline in this region (see Fig. 10d) through coastal Kelvin wave propagation from the equatorial

region. In contrast, the influence of IOD along the Omani coast is almost negligible (Fig. 10d), and oxygen variations here seem to be related to offshore Ekman pumping (not shown). Further dedicated studies are needed to better understand the oxygen variability in these sensitive regions and their potential impacts on the ecosystem and fisheries.

Acknowledgements

This work is a part of the CSIR-funded INDIAS IDEA project. We thank CSIR-NIO data centre and Chemical Oceanography Division for making the archived cruise and CaTS data available for the present study. M. Lengaigne, C. Ethé, J. Vialard and M. Levy benefited from Institut de Recherche pour le Développement (IRD) funding for their visits to the CSIR-NIO. We thank the NEMO-PISCES modelling team. The authors also thank IFCPAR (Indo French Centre for Promotion of Advanced Research), New Delhi for funding of the proposal 4907-1 that contribute to the present research. The simulations were performed on HPC Pravah at CSIR-NIO. V. Parvathi is funded by CSIR under Senior Research Fellowship. V. Parvathi and I. Suresh acknowledge the support rendered by T. Pankajakshan and P. Vethamony, and acknowledge M. Afroosa for assistance in data processing. This is NIO contribution number XXXX.

References

Akhil, V. P., Lengaigne, M., Vialard, J., Durand, F., Keethi, M. G., Chaitanya, A. V. S., Papa, F., de Boyer Montégut, C.: A modelling study of the processes controlling the Bay of Bengal Sea Surface Salinity interannual variability, Submitted to JGR Oceans, 2016.

Akhil, V. P., Durand, F., Lengaigne, M., Vialard, J., Keethi, M. G., Gopalakrishna, V. V., Deltel, C., Papa, F., de Boyer Montégut, C.: A modelling study of the processes of surface salinity seasonal cycle in the Bay of Bengal, J. Geophys. Res., 116, 3926-3947, doi:10.1002/2013JC009632, 2014.

Arntz, W. E., Gallardo, V. A., Gutierrez, D., Isla, E., Levin, L. A., Mendo, J., Neira, C., Rowe, G. T., Tarazona, J., and Wolff, M.: El Niño and similar perturbation effects on the benthos of the Humboldt, California, and Benguela Current upwelling ecosystems, Adv. Geosci., 6, 243–265, 2006.

Annamalai, H., Murtugudde, R., Potemra, J., Xie, S. P., Liu, P., Wang, B.: Coupled dynamics over the Indian Ocean: spring initiation of the zonal mode, Deep Sea Res II 50:2305–2330, 2003.

Aparna, S. G., McCreary, J. P., Shankar, D., and Vinayachandran, P. N.: Signatures of Indian ocean dipole and El Niño-Southern oscillation events in sea level variations in the Bay of Bengal, J. Geophys. Res., 117, C10012, doi:10.1029/2012JC008055, 2012.

Aumont, O. and Bopp, L.: Globalizing results from ocean in situ iron fertilization studies, Global Biogeochem. Cy., 20, GB2017, doi:10.1029/2005GB002591, 2006.

Biogeosciences Discuss., doi:10.5194/bg-2016-195, 2016
Manuscript under review for journal Biogeosciences
Published: 9 June 2016

Aumont, O., Ethé, C., Tagliabue, A., Bopp, L., and Gehlen, M.: PISCES-v2: an ocean biogeochemical model for carbon and ecosystem studies. Geoscientific Model Development, 8(8), 2465-2513, 2015.

Banse, K.: On upwelling and bottom-trawling off the south west coast of India, J. Mar. Biol. Assoc. India, 1, 33–49, 1959.

Barnier, B., Madec, G., Penduff, T., Molines, J., Treguier, A., Sommer, J. L., Beckmann, A., Biastoch, A., Boning, C., Dengg, J.,Derval, C., Durand, E., Gulev, S., Remy, E., Talandier, C., Theetten, S., Maltrud, M., McClean, J., and Cuevas, B. D.: Impact of partial steps and momentum advection schemes in a global ocean circulation model at eddy permitting resolution, Ocean Dynam.,56, 543–567, doi:10.1007/s10236-006-0082-1, 2006.

Brodeau, L., Barnier, B., Penduff, T., Treguier, A.-M., and Gulev, S.: An ERA40 based atmospheric forcing for global ocean circulation models, Ocean Model., 31, 88–104, doi:10.1016/j.ocemod.2009.10.005, 2009.

Boyer, T. P., Antonov, J. I., Baranova, O. K., Coleman, C., Garcia, H. E., Grodsky, A., Johnson, D. R., Locarnini, R. A., Mishonov, A. V., O'Brien, T. D., Paver, C. R., Reagan, J. R., Seidov, D., Smolyar, I. V., and Zweng, M. M.: World Ocean Database 2013, NOAA Atlas NESDIS 72, S. Levitus, Ed., A. Mishonov, Technical Ed.; Silver Spring, MD, 209 pp., 2013.

Currie, J., Lengaigne, M., Vialard, J., Kaplan, D., Aumont, O., Maury, O.: Indian Ocean Dipole and El Niño/Southern Oscillation impacts on regional chlorophyll anomalies in the Indian Ocean. Biogeosciences 10:5841–5888, 2013.

Carruthers, J. N., Gogate, S. S., Naidu, J. R., and Laevastu, T.: Shoreward upslope of the layer of minimum oxygen off Bombay: Its influence on marine biology, especially fisheries, Nature, 183,1084–1087, 1959.

Diaz, R. J. and Rosenberg, R.: Spreading dead zones and consequences for marine ecosystems., Science, 321, 26–29, 2008.

Dussin, R., Treguier A.-M., Molines, J. M., Barnier, B., Penduff, T., Brodeau, L., Madec, G.: Definition of the interannual experiment ORCA025-B83, 1958–2007, LPO Report 902, 2009.

Eilola, K., Meier, H. E. M., and Almroth, E.: On the dynamics of oxygen, phosphorus and cyanobacteria in the Baltic Sea: A model study, J. Marine Syst., 75, 163–184, doi:10.1016/j.jmarsys.2008.08.009, 2009.

Fukumori, I., Raghunath, R., and Fu, L.: Nature of global large scale sea level variability in relation to atmospheric forcing: A modeling study, J. Geophys. Res., 103(C3), 5493-5512, 1998.

Geider, R. J., MacIntyre, H. L., and Kana, T. M.: A dynamic regulatory model of phytoplanktonic acclimation to light, nutrients, and temperature, Limnol. Oceanogr., 43, 679–694, 1998.

Gregoire, M. and Friedrich, J.: Nitrogen budget of the northwestern Black Sea shelf as inferred from modeling studies and in-situ benthic measurements, Mar. Ecol.-Prog. Ser., 270, 15–39, 2004.

Gupta, G. V. M., Sudheesh, V., Sudharma, K. V., Saravanane, N., Dhanya,V., Dhanya, K. R., Lakshmi, G., Sudhakar, M., and Naqvi, S. W. A.: Evolution to decay of upwelling and associated biogeochemistry over the southeastern Arabian Sea shelf, J. Geophys. Res. Biogeosci., 121,159-175, doi:10.1002/2015JG003163, 2016.

Gutierrez, D., Enriquez, E., Purca, S., Quipuzcoa, L., Marquina, R., Flores, G., and Graco, M.: Oxygenation episodes on the continental shelf of central Peru: Remote forcing and benthic ecosystem response, Prog. Oceanogr., 79, 177–189, 2008.

Helly, J. J. and Levin, L. A.: Global distribution of naturally occurring marine hypoxia on continental margins, Deep-Sea Res. I, 51, 1159–1168, 2004.

Hetland, R. and DiMarco, S.: How does the character of oxygen demand control the structure of hypoxia on the Texas-Louisiana continental shelf?, J. Mar. Syst., 70, 49–62, doi:10.1016/j.jmarsys.2007.03.002, 2008.

Jensen, T. G.: Arabian Sea and Bay of Bengal exchange of salt and tracers in an ocean model. Geophys. Res. Lett., 28(20), 3967–3970, doi:10.1029/2001GL013422, 2001.

Keerthi, M.G., Lengaigne, M., Drushka, K., Vialard, J., de Boyer Montégut, C., Pous, S., Levy, M., and Muraleedharan, P. M.: Intraseasonal variability of mixed layer depth in the tropical Indian, Clim. Dyn., doi:10.1007/s00382-015-2721-z, 2015.

Koné, V., Aumont, O., Lévy, M., and Resplandy, L.: Physical and Bio-geochemical controls of the Phytoplankton Seasonal Cycle in the Indian Ocean: a modeling study. in: Wiggert J. D., Hood, R. R., Naqvi, S. W. A., Brink, K. H., and Smith, S. L., 185, 147–166, American Geophysical Union, Washington DC, USA, 2009.

Krishnakumar, P. K. and Bhat, G. S.: Seasonal and interannual variations of oceanographic conditions off Mangalore coast (Karnataka, India) in the Malabar upwelling system during 1995–2004 and their influences on the pelagic fishery.Fisheries Oceanography, 17 (1). pp. 45-60, 2008.

Large, W. G., Yeager, S. G.: Diurnal to decadal global forcing for ocean and sea-ice models: the data sets and flux climatologies. NCAR/TN-460 STR, 111 pp, 2004.

Lengaigne, M., Menkes, C., Aumont, O., Gorgues, T., Bopp, L., Andre, J. M., Madec, G.: Influence of the oceanic biology on the tropical Pacific climate in a coupled general circulation model. Climate Dynamics 28, 503–516, 2007.

Levy, M., Shankar, D., Andre, J. M., Shenoi S. S. C., Durand, F., de Boyer, C., Montegut, C.: Basinwide seasonal evolution of the Indian Ocean's phytoplankton blooms. J Geophys Res 112:C12014, 2007.

Lee, C. M., Jones, B. H., Brink, K. H., Fischer, A. S.: The upper ocean response to monsoonal forcing in the Arabian Sea: seasonal and spatial variability. Deep Sea Res Part II 47:1177–1226, 2000.

Luo, J. J., Masson, S., Behera, S., and Yamagata, T.: Experimental forecasts of the Indian Ocean dipole using a coupled OAGCM. J. Climate, 20, 2178–2190, 2007.

Luo, J. J., Behera, S., Masumoto, Y., Sakuma, H., and Yamagata, T.: Successful prediction of the consecutive IOD in 2006 and 2007, Geophys. Res. Lett., 35, L14S02, doi:10.1029/2007GL032793, 2008.

Madec, G.: NEMO, the ocean engine, Note du Pole de modelisation, Institut Pierre-Simon Laplace (IPSL), France, No 27 ISSN No 1288–1619, available at: "http://www.nemo-ocean.eu/About-"www.nemo-ocean.eu/About-NEMO/Reference-manuals, 2008.

Madhupratap, M., Kumar, S. P., Bhattathiri, P. M. A., Kumar, M. D., Raghukumar, S., Nair, K. K. C., and Ramaiah, N.: Mechanism of the biological response to winter cooling in the northeastern Arabian Sea, Nature, 384, 549–552, 1996.

Maya, M. V., Karapurkar, S. G., Naik, H., Roy, R., Shenoy, D. M., and Naqvi, S. W. A.: Intra-annual variability of carbon and nitrogen stable isotopes in suspended organic matter in waters of the western continental shelf of India. Biogeosciences, 8, 3441–3456, doi:10.5194/bg-8-3441-2011, 2011.

McCreary, J. P., Kundu, P. K., and Molinari, R. L.: A numerical investigation of dynamics, thermodynamics and mixed-layer processes in the Indian Ocean, Progr. Oceanogr., 31, 181–244,doi:10.1016/0079-6611(93)90002-U, 1993.

McCreary, J. P., Yu, Z., Hood, R., Vinaychandran, P. N., Furue, R., Ishida, A., and Richards, K.: Dynamics of the Indian-Ocean oxygen minimum zones, Progr. Oceanogr., 2013.

Monteiro, P. M. S., Van der Plas, A. K., Melice, J.-L., and Florenchie, P.: Interannual hypoxia variability in a coastal upwelling system: Ocean–shelf exchange, climate and ecosystem-state implications. Deep-Sea Res. Pt. I, 435–450, 2008.

Morales, C. E., Hormazabal, S.E., and Blanco, J. L.: Interannual variability in the mesoscale distribution of the depth of the upper boundary of the oxygen minimum layer off northern Chile (18-24S): implications for the pelagic system and biogeochemical cycling. Journal of Marine Research, 57, pp. 909–932, 1999.

Morrison, J. M., Codispoti, L. A., Smith, S. L., Wishner, K., Flagg, C., Gardner, W. D., Gaurin, S., Naqvi, S. W. A., Manghnani, V., Prosperie, L., and Gundersen, J. S.: The oxygen minimum zone in the Arabian Sea during 1995 - overall seasonal and geographic patterns, and relationship to oxygen gradients, Deep-Sea Res. Pt.II, 46, 1903–1931, doi:10.1016/S0967-0645(99)00048-X, 1999.

Murtugudde, R., McCreary, J. P., and Busalacchi, A. J.: Oceanic processes associated with anomalous events in the Indian Ocean with relevance to 1997–1998, J. Geophys. Res., 105, 3295–3306, 2000.

Naqvi, S.W.A.: Some aspects of the oxygen-deficient conditions and denitrification in the Arabian Sea, J. Mar. Res., 45, 1049-1072, 1987.

Naqvi, S. W. A, Naik, H., Jayakumar, D. A., Pratihary, A. K., Narvenkar, G., Kurian, S., Agnihotri, R., Shailaja, M. S., and Narvenkar, P. V.: Seasonal anoxia over the Western Indian continental shelf, Geophysical Monograph Series, 185,10.1029/2008GM000745, 2009.

Naqvi, S. W. A., Jayakumar, D. A., Narvekar, P. V., Naik, H., Sarma, V.V. S. S., D'Souza, W., Joseph, S., and George, M. D.: Increased narine production of N2O due to intensifying anoxia on the Indian continental shelf, Nature, 408, 346-349, 2000.

Naqvi, S. W. A., Bange, H. W., Farías, L., Monteiro, P. M. S., Scranton, M. I., and Zhang, J.: Marine hypoxia/anoxia as a source of CH_4 and N_2O, Biogeosciences, 7, 2159-2190, doi:10.5194/bg-7-2159-2010, 2010a.

Naqvi, S. W. A., Moffett, J. W., Gauns, M. U., Narvekar, P. V., Pratihary, A. K., Naik, H., Shenoy, D. M., Jayakumar, D. A., Goepfert, T. J., Patra, P. K., Al-Azri, A., and Ahmed, S. I.: The Arabian Sea as a high-nutrient, low-chlorophyll region during the late Southwest Monsoon, Biogeosciences, 7, 2091–2100, 2010, doi:10.5194/bg-7-2091, 2010b.

Naqvi, S. W. A., Naik, H., Pratihary, A. K., D'Souza, W., Narvekar, P. V., Jayakumar, D. A., Devol, A. H., Yoshinari, T., and Saino, T.: Coastal versus open-ocean denitrification in the Arabian Sea, Biogeosciences, 3, 621–633, doi:10.5194/bg-3-621-2006, 2006.

Nisha, K., Lengaigne, M., Gopalakrishna, V. V., Vialard, J., Pous, S., Peter, A-C., Durand, F., Naik, S.: Processes of summer intraseasonal sea surface temperature variability along the coasts of India, Ocean Dynamics, 63, 329-346, 2013.

Pena, M. A., Katsev, S., Oguz, T., Gilbert, D.: Modeling dissolved oxygen dynamics and hypoxia Biogeosciences, 7 (3), pp. 933–957, 2010.

Pillai, V. N., Pillai, V. K., Gopinathan, C. P., and Nandakumar, A.: Seasonal variations in the physical, chemical and biologicalcharacteristics of the eastern Arabian Sea, J. mar. biol. Ass. India, 42 (1&2) : 1 – 20, 2000.

Piontkovski, S. A., and H.S. AL-Oufi: The Omani shelf hypoxia and the warming Arabian Sea, International Journal of Environmental Studies, doi:10.1080/00207233.2015.1012361, 2015.

Praveen Kumar B., Vialard, J., Lengaigne, M., Murty, V. S. N., Foltz, G., McPhaden, M. J., Pous, S., and de Boyer Montégut, C.: Processes of interannual mixed layer temperature variability in the Thermocline Ridge of the Indian Ocean, Clim. Dyn., 43, 2377-2397, 2014.

Resplandy, L., Levy, M., Madec, G., Pous, S., Aumont, O., and Kumar, D.: Contribution of mesoscale processes to nutrient budgets in the Arabian Sea, J. Geophys. Res., 116, C11007, doi:10.1029/2011JC007006, 2011.

Resplandy, L., Lévy, M., Bopp, L., Echevin, V., Pous, S., Sarma, V. V. S. S., and Kumar, D.: Controlling factors of the oxygen balance in the Arabian Sea's OMZ, Biogeosciences, 9, 5095–5109, doi:10.5194/bg-9-5095-2012, 2012.

Resplandy, L., Vialard, J., Lévy, M., Aumont, O., and Dandonneau. Y. : Seasonal and intraseasonal biogeochemical variability in the thermocline ridge of the southern tropical Indian Ocean,J. Geophys. Res.,114, C07024,doi:10.1029/2008JC005246, 2009.

Saji, N. H., Goswami, B. N., Vinayachandran, P. N., Yamagata, T.: A dipole mode in the tropical Indian Ocean. Nature 401:360–363, 1999.

Sarma, V. V. S. S.: An evaluation of physical and biogeochemical processes regulating perennial suboxic conditions in the water column of the Arabian Sea, Global Biogeochem. Cy., 16, 1082, doi:10.1029/2001GB001461, 2002.

Sarma, V. V. S. S., Sridevi, B., Maneesha, K., Sridevi, T., Naidu, S.A., et al.: Impact of atmospheric and physical forcings on biogeochemical cycling of dissolved oxygen and nutrients in the coastal Bay of Bengal. J. Oceanogr., 2013.

Satya Prakash, Prince Prakash and Ravichandran, M.: Can oxycline depth be estimated using sea level anomaly (SLA) in the northern Indian Ocean?, Remote Sensing Letters, 4:11, 1097-1106, DOI: 10.1080/2150704X.2013.842284, 2013.

Shankar, D., Vinayachandran, P. N., and Unnikrishnan, A. S.: The monsoon currents in the north Indian Ocean, Prog. Oceanogr., 52, 63–120, 2002.

Shetye, S. R., Gouveia, A. D., Shenoi, S. S. C., Sundar, D., Michael, G. S., Almeida, A. M., and Santanam, K.: Hydrography and circulation off the West coast of India during the Southwest monsoon 1987, J. Mar. Res., 48, 359–378, 1990.

Shi, L., Hendon, H. H., Alves, O., Luo, J–J., Balmaseda, M. and Anderson, D.: How predictable is the Indian Ocean Dipole? Mon. Weather Rev., 140:3867–3884, 2012.

Smitha, B. R., Sanjeevan, V. N., Vimalkumar, K. G., Revichandran, C.: On the upwelling off the southern tip and along the west coast of India, J. Coast. Res., 24(3):95-102, 2008.

Sooraj, K. P., Annamalai, H., Kumar, A., and Wang, H.: A comprehensive assessment of CFS seasonal forecast over the tropics. Wea. Forecasting, 27, 3–27, 2012.

Suresh, I., Vialard, J., Izumo, T., Lengaigne, M., Han, W., McCreary, J., Muraleedharan, P.M.: Dominant role of winds near Sri Lanka in driving seasonal sea-level variations along the west Indian coast, (sumbitted to GRL), 2016.

Takahashi, T., Broecker, W. S., and Langer, S.: Redfield ratio based on chemical data from isopycnal surfaces, J. Geophys. Res., 90,6907–6924, 1985.

Treguier, A.M., Barnier, B., de Miranda, A. P., Molines, J. M., Grima, N., Imbard, M., Madec, G., Messager, C., Reynaud, T. and Michel, S.: An eddy-permitting model of the Atlantic circulation: Evaluating open boundary conditions, J. Geophys. Res., 106, C10, 22,115-22,129, 2001.

Uppala, S. M., KÅllberg, P. W., Simmons, A. J., Andrae, U., Bechtold, V. D. C., Fiorino, M., Gibson, J. K., Haseler, J., Hernandez, A., Kelly, G. A., Li, X., Onogi, K., Saarinen, S., Sokka, N., Allan, R., Andersson, E., Arpe, K., Balmaseda, M., Beljaars, A., van de Berg, L., Bidlot, J., Bormann, N., Caires, S., Chevallier, F., Dethof, A., Dragosavac, M., Fisher, M., Fuentes, M., Hagemann, S., Holm, E., Hoskins, B., Isaksen, L., Janssen, P., Jenne, R., McNally, A., Mahfouf, J.-F., Morcrette, J.-J., Rayner, N., Saunders, R., Simon, P., Sterl, A., Trenberth, K., Untch, A., Vasiljevic, D., Viterbo, P., and Woollen, J.: The ERA-40 re-analysis, Q. J. Roy. Meteor. Soc., 131, 2961–3012, 2005.

Valcke, S.: The OASIS3 coupler: A European climate modelling community software, Geosci. Model Dev., 6(2), 373–388, doi:10.5194/ gmd-6-373-2013, 2013.

Vaquer-Sunyer, R., Duarte, C.M.: Thresholds of hypoxia for marine biodiversity. Proc. Natl. Acad. Sci. 105, 15452–15457, 2008.

Vialard, J., Drushka, K., Bellenger, H., Lengaigne, M., Pous, S., Duvel, J-P.: Understanding Madden–Julian-induced sea surface temperature variations in the North Western Australian Basin. Clim Dyn. doi:10.1007/s00382-012-1541-7, 2013.

Wang, L. and Justic, D.: A modeling study of the physical processes affecting the development of seasonal hypoxia over the inner Louisiana-Texas shelf: Circulation and stratification, Cont.Shelf Res., 29, 1464–1476, 2009.

Webster, P. J., Moore, A. M., Loschnigg, J. P., Leben, R. R.: Coupled ocean atmosphere dynamics in the Indian Ocean during 1997-98.Nature 401:356–360, 1999.

Wiggert, J. D., Murtugudde, R., and McClain, C. R.: Processes controlling interannual variations in wintertime (northeast monsoon) primary productivity in the central Arabian Sea, Deep Sea Res., Part II, 47,2319 – 2343, 2002.

Wiggert, J. D., Hood, R., Banse, K., and Kindle, J.: Monsoon driven biogeochemical processes in the Arabian Sea, Progr. Oceanogr., 65, 176–213, doi:10.1016/j.pocean.2005.03.008, theArabian Sea of the 1990s: New Biogeochemical Understanding, 2005.

Wiggert, J. D., Vialard, J., and Behrenfeld, M. J.: Basinwide modification of dynamical and biogeochemical processes by the positive phase of the Indian Ocean Dipole during the SeaWiFS era, in: Indian Ocean Biogeochemical Processes and Ecological Variability, vol. 185, edited by: J. D. Wiggert, R. R. Hood, S. Wajih, A. Naqvi, K. H. Brink, and S. L. Smith, p. 350, 2009.

Zhang, Y. C., Rossow, W. B., Lacis, A. A., Oinas, V., Mishchenko, M. I.: Calculation of radiative fluxes from the surface to top of atmosphere based on ISCCP and other global data sets: refinments of the radiative transfer model and the input data. J Geophys Res 109:D19105. doi:10.1029/2003JD004457, 2004.

Zhao, M., and Hendon, H. H.: Representation and prediction of the Indian Ocean dipole in the POAMA seasonal forecast model. Quart. J. Roy. Meteor. Soc., 135, 337–352, 2009.

Biogeosciences Discuss., doi:10.5194/bg-2016-195, 2016
Manuscript under review for journal Biogeosciences
Published: 9 June 2016

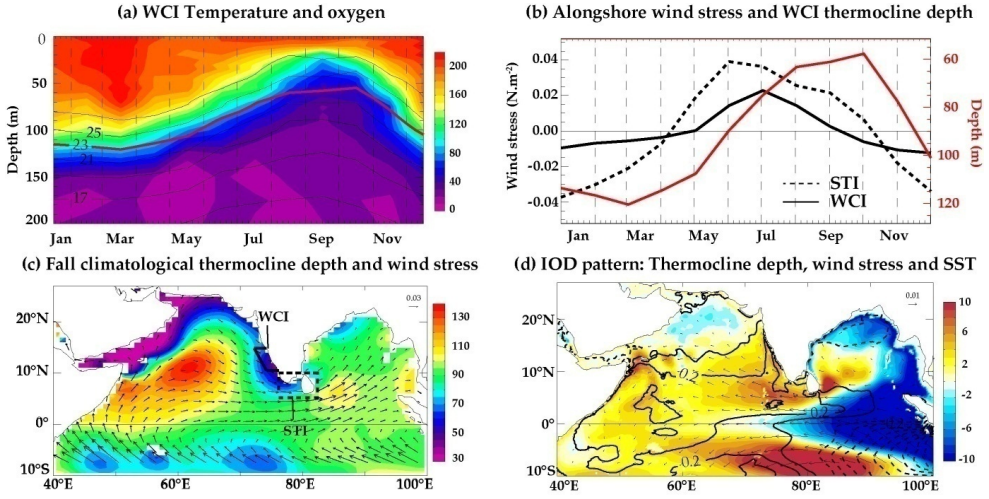

Figure 1.(a) Observed (WOA13) seasonal climatology of oxygen (µmol.l^{-1}; shaded) and temperature (°C; contour) vertical distribution in the WCI box (displayed on panel **c**). **(b)** Seasonal climatology of the WCI 23°C isotherm (red curve) and alongshore wind stress in the WCI box (plain black curve) and at the southern tip of India (STI; dashed black curve). Upwelling-favourable winds are displayed as positive. **(c)** September-November climatological thermocline depth (m; shaded) and wind stress (N.m^{-2}) over the northern Indian Ocean. The thick (dashed) black frame indicates the boundary of the WCI (STI) box. **(d)** Anomalies of thermocline depth (m; shaded), SST (°C; contour, with dashed contours indicating negative values) and wind stress (N.m^{-2}; vectors) associated with the occurrence of a positive Indian Ocean Dipole in the northern Indian Ocean (see Figure 10 and related text for details).

Biogeosciences Discuss., doi:10.5194/bg-2016-195, 2016
Manuscript under review for journal Biogeosciences
Published: 9 June 2016

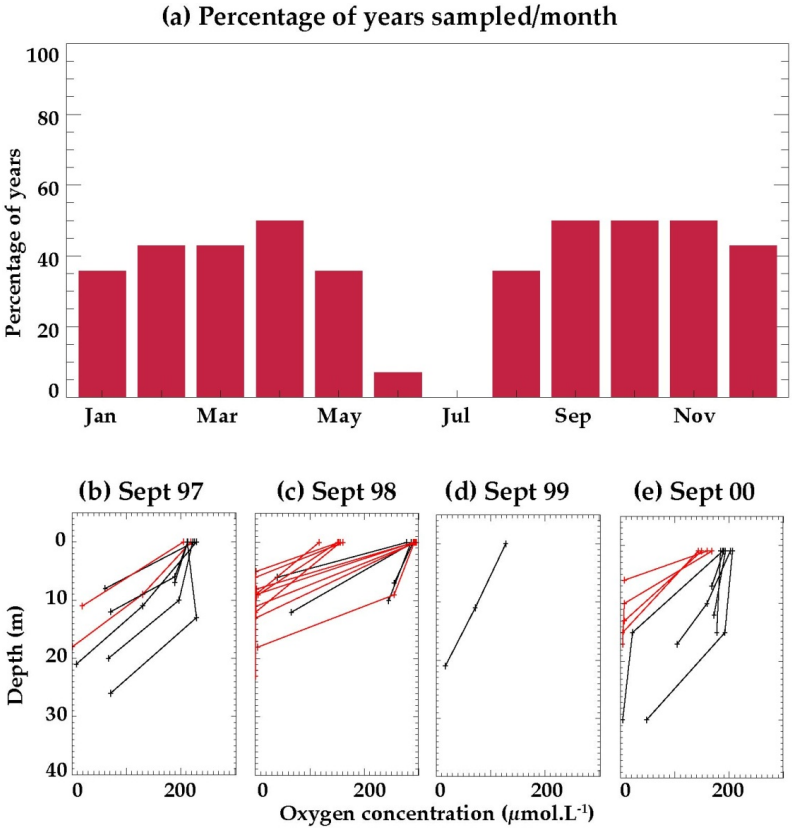

Figure 2. (a) Histogram of the percentage of years sampled for each calendar month over the 1997-2010 period at CaTS station. Vertical oxygen profiles collected at CaTS in September **(b)** 1997, **(c)** 1998, **(d)** 1999 and **(e)** 2000. Profiles with oxygen concentrations below 20 μmol.l^{-1} within the top 20 m of the water column are indicated in red

5

Biogeosciences Discuss., doi:10.5194/bg-2016-195, 2016
Manuscript under review for journal Biogeosciences
Published: 9 June 2016

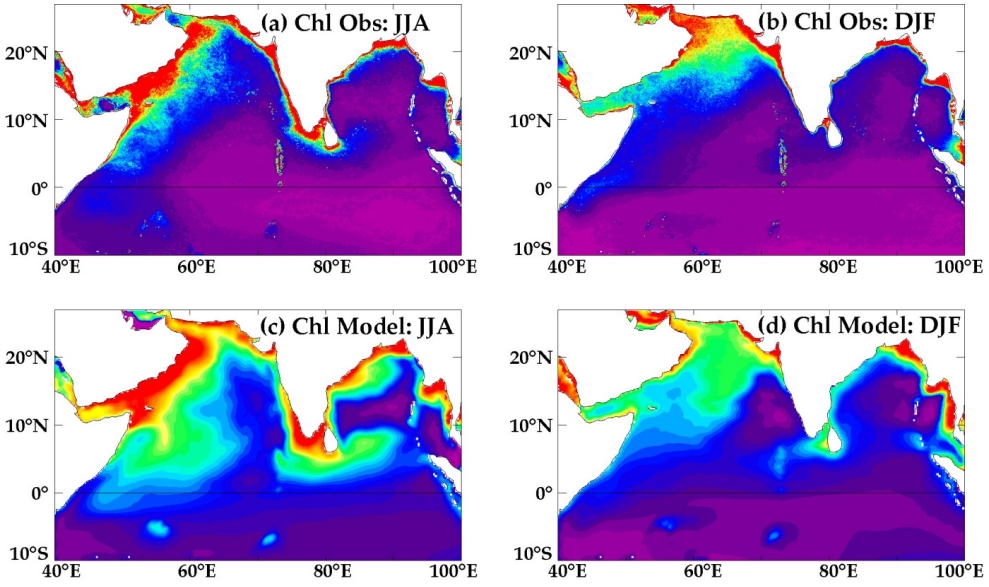

Figure 3. Northern Indian Ocean surface chlorophyll (mg.m^{-3}) climatology for (left) summer (June-August) and (right) winter (December-February) in (top) the ESA satellite product and (bottom) model.

Biogeosciences Discuss., doi:10.5194/bg-2016-195, 2016
Manuscript under review for journal Biogeosciences
Published: 9 June 2016

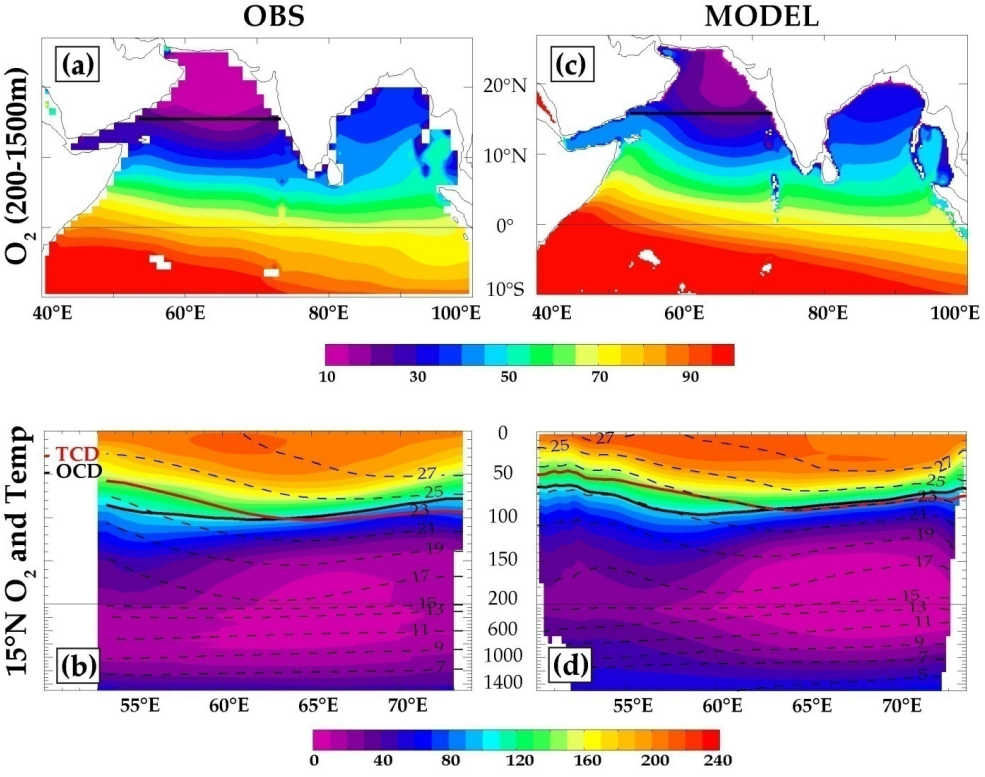

5 **Figure 4.(a)** Map of yearly climatological O_2 concentration (μmol.l^{-1}) averaged between 200 and 1500-m depths in the northern Indian Ocean from WOA13. **(b)** East-West section at 15°N in the Arabian Sea (marked as thick black line in panels a and c) of yearly climatological O_2 (μmol.l^{-1}; shaded) and temperature (°C; dashed contours) vertical distribution from WOA13. **(c, d)** Same as **(a,b)** but for the model. Depths of 23° C isotherm (red) and of 100 μmol.l^{-1} isoline (thick black) are marked on panels **b** and **d.**

10

Biogeosciences Discuss., doi:10.5194/bg-2016-195, 2016
Manuscript under review for journal Biogeosciences
Published: 9 June 2016

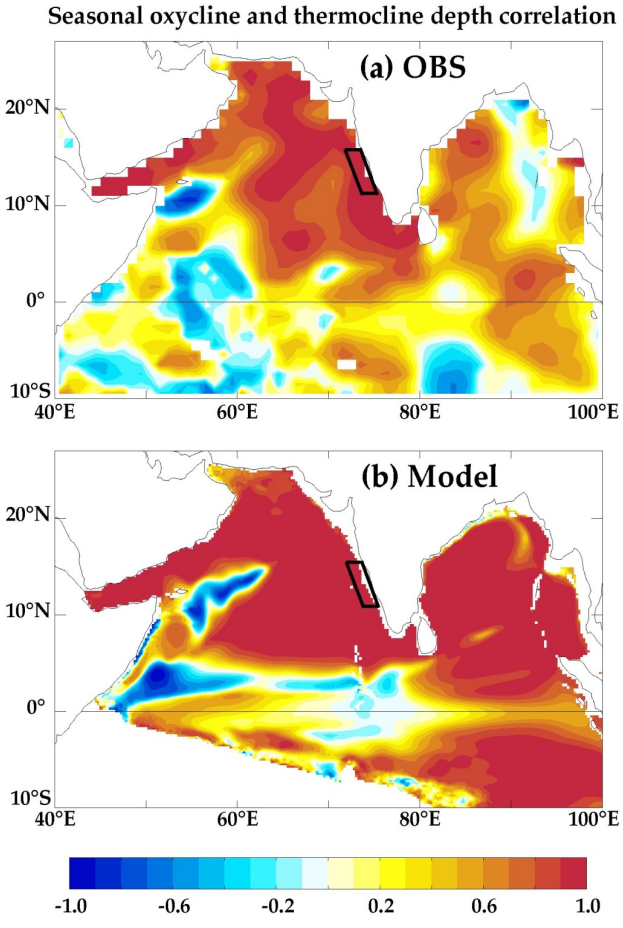

Figure 5. Maps of correlation between the mean seasonal cycle of oxycline and thermocline depths over the northern Indian Ocean from **(a)** WOA13 and **(b)** model. Values are masked when the oxycline could not be defined, i.e., when the oxygen concentration is above 100 μmol.l^{-1} in the entire water column. The WCI box boundaries are indicated on each panel.

Biogeosciences Discuss., doi:10.5194/bg-2016-195, 2016
Manuscript under review for journal Biogeosciences
Published: 9 June 2016

Biogeosciences Discussions
Open Access
EGU

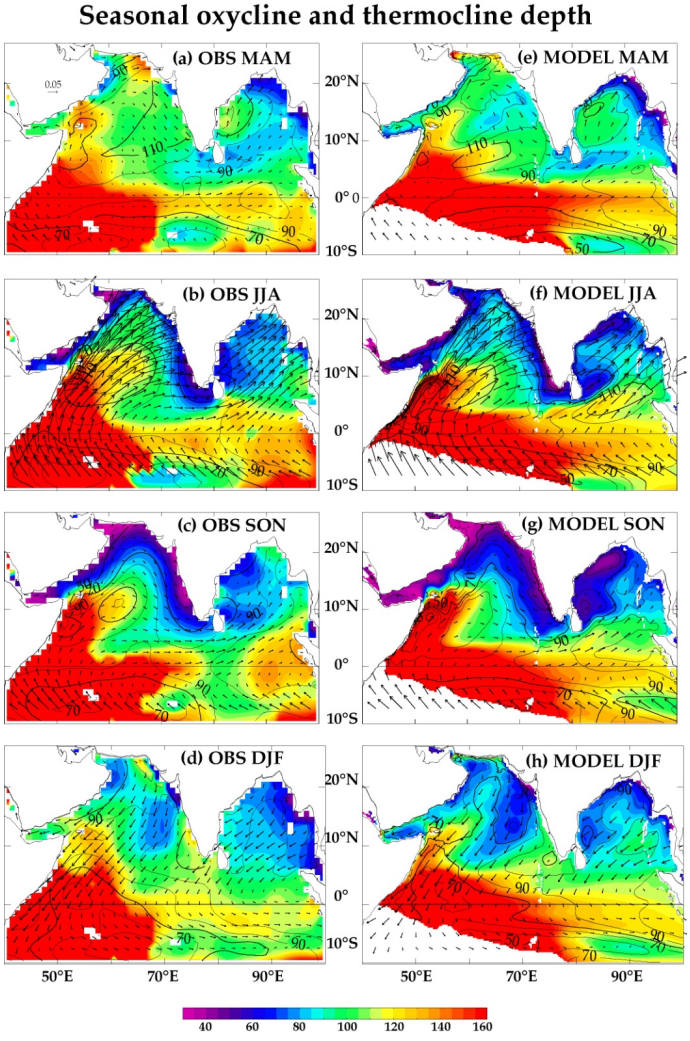

Figure 6. Maps of the seasonal climatology of oxycline depth (m; shaded), thermocline depth (m; contours) for WOA13 in **(a)** March-May, **(b)** June-August, **(c)** September-November and **(d)** December-February. **(e-h)** Same as **(a-d)**, but from the model. Seasonal wind stress ($N.m^{-2}$) pattern from the model forcing are also shown as vectors on all panels.

Biogeosciences Discuss., doi:10.5194/bg-2016-195, 2016
Manuscript under review for journal Biogeosciences
Published: 9 June 2016

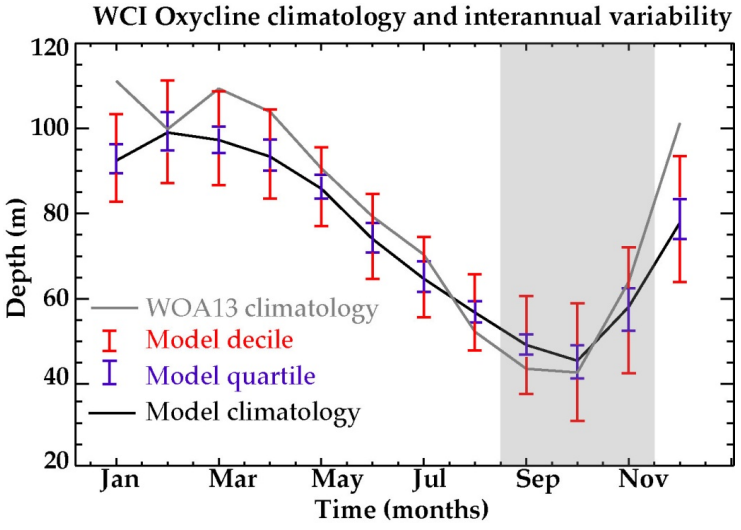

Figure 7. Monthly climatology of the oxycline depth from WOA13 and model in WCI box (indicated as black frames on Fig. 4). The upper and lower quartiles and deciles of the model monthly distributions are also shown to illustrate the interannual variability around the mean value.

Biogeosciences Discuss., doi:10.5194/bg-2016-195, 2016
Manuscript under review for journal Biogeosciences
Published: 9 June 2016

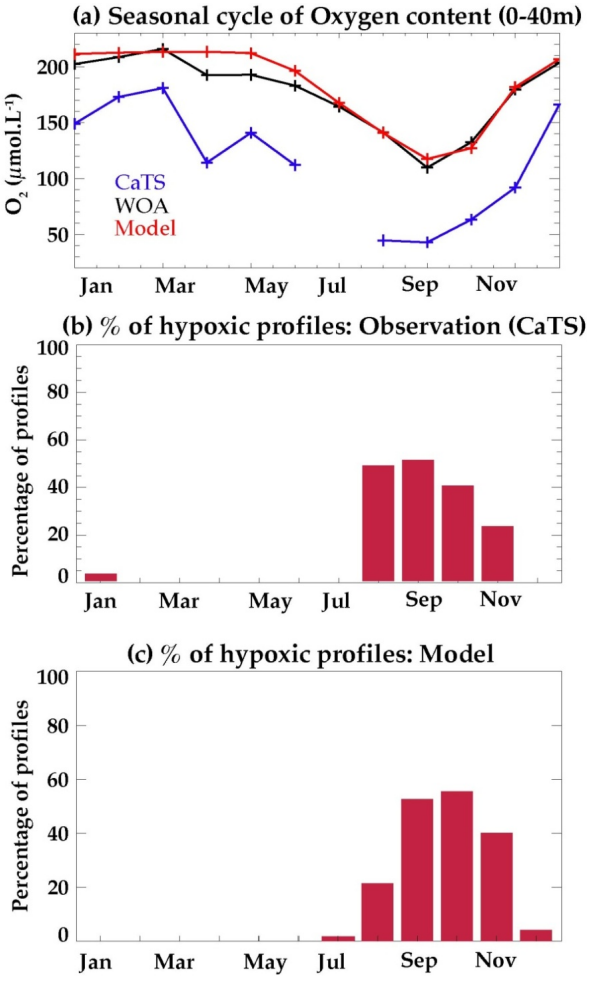

Fig. 8. (a) Monthly climatological time series of upper ocean oxygen content (0-40 m depth averaged) from the model, WOA13 in the WCI box and from the in-situ CaTS data. Percentage of profiles for each calendar month for which **(b)** oxygen concentrations below 20 µmol.l^{-1} occur within the top 20 m in CaTS data and **(c)** where oxygen concentrations below 80 µmol.l^{-1} occur within the top 50 m from the model at WCI box.

Biogeosciences Discuss., doi:10.5194/bg-2016-195, 2016
Manuscript under review for journal Biogeosciences
Published: 9 June 2016

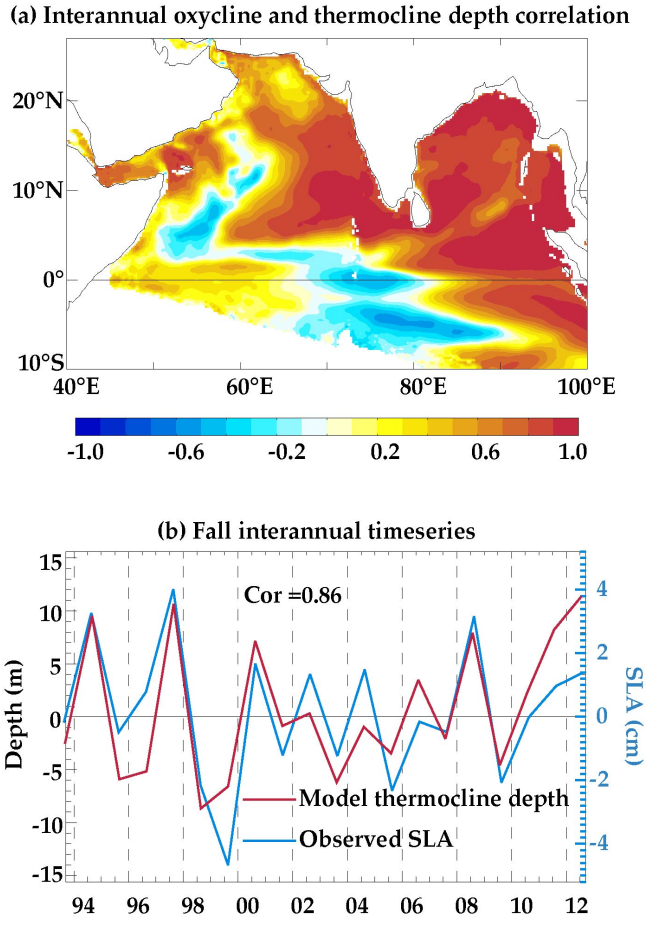

Figure 9. (a) Map of correlation between the modelled oxycline and thermocline depth interannual anomalies. **(b)** Fall (September-November) WCI box (see frame on panel a) averaged interannual anomalies of the model thermocline depth (red line) and altimetry-derived sea-level anomalies (blue line). On panel a, values are masked when the oxycline and/or thermocline could not be defined for more than 20% of the profiles at a given location.

Biogeosciences Discuss., doi:10.5194/bg-2016-195, 2016
Manuscript under review for journal Biogeosciences
Published: 9 June 2016

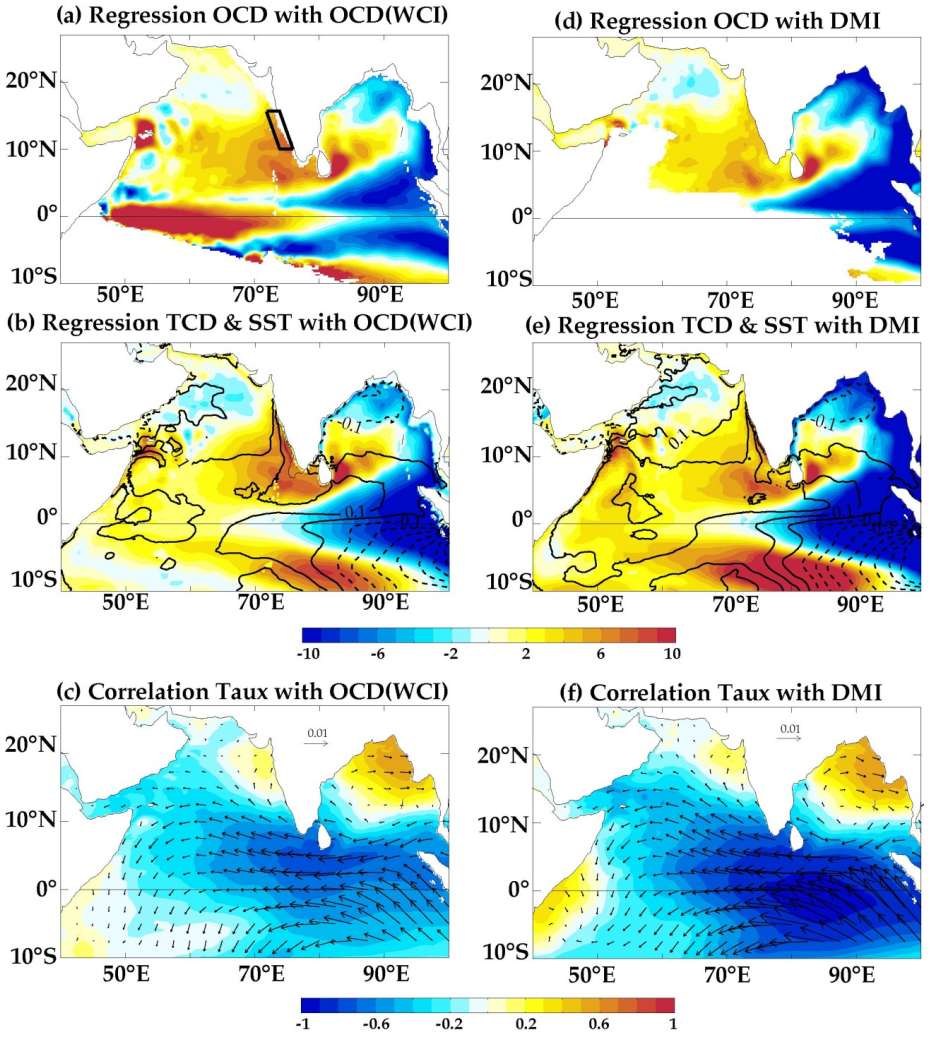

Figure 10. Maps of regression coefficients of boreal fall (SON) interannual **(a)** oxycline (m; shaded), **(b)** thermocline (m; shaded) and SST (^{o}C; contours) and **(c)** wind stress anomalies (N.m^{-2}; vectors) to normalized oxycline interannual anomalies averaged over WCI box (marked in panel a). Colours on panel (c) indicate the correlation between zonal wind stress anomalies and WCI-averaged oxycline interannual anomalies. **(d-f)** Same as **(a-c)** but regressed to the fall DMI index.

Biogeosciences Discuss., doi:10.5194/bg-2016-195, 2016
Manuscript under review for journal Biogeosciences
Published: 9 June 2016

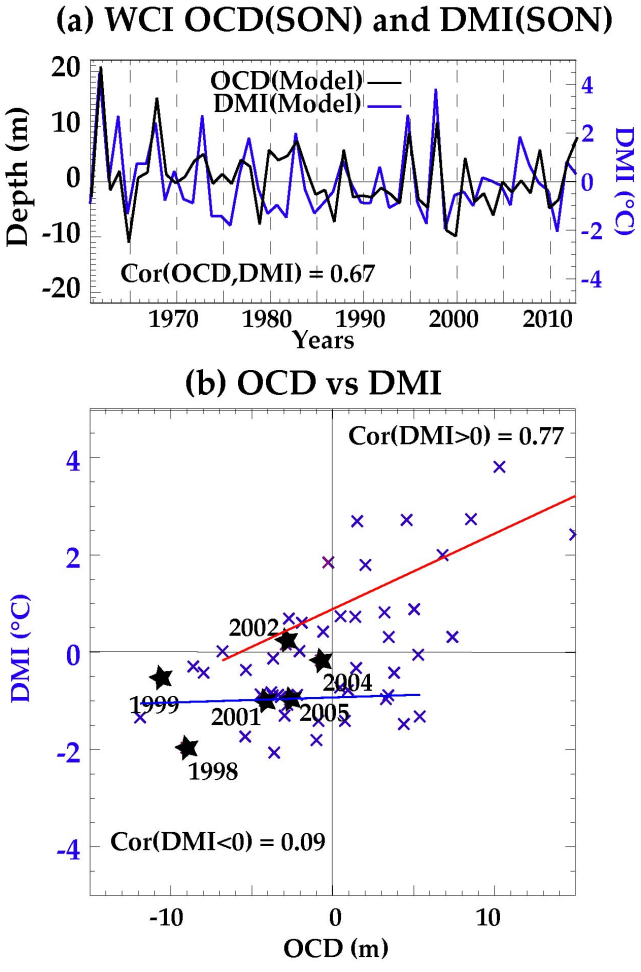

Fig. 11. (a) Time series of WCI SON-averaged interannual anomalies of modelled oxycline depth (black) and SON DMI (blue). **(b)** Scatterplot of the fall interannual anomalies of WCI oxycline depth vs. DMI. The correlation coefficient between the oxycline and DMI timeseries is displayed on panel a. Solid red and blue lines on panel b respectively represent regression slopes fitted separately for positive and negative DMI values. Anoxic events reported by Naqvi et al. (2009) are marked as black stars and the corresponding years are displayed.

Biogeosciences Discuss., doi:10.5194/bg-2016-195, 2016
Manuscript under review for journal Biogeosciences
Published: 9 June 2016

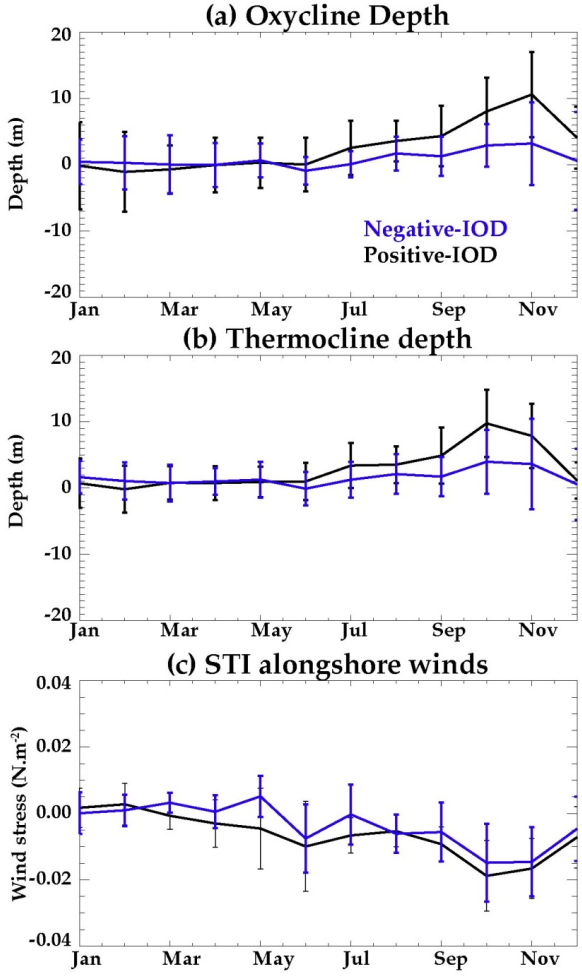

Figure 12. Seasonal evolution of composites of **(a)** WCI OCD, **(b)** WCI TCD and **(c)** STI alongshore wind stress during positive (black) and negative (blue) IOD events. Positive (negative) IODs are defined when the DMI averaged for SON season is greater (less) than 1° C. The whiskers indicate the 95% confidence interval on the composited value. Positive IOD events considered in this composite are years 1961, 1963, 1967, 1972, 1977, 1982, 1994, 1997, and 2006 while negative ones are 1964, 1973, 1974, 1975, 1979, 1981, 1984, 1992, 1996, 1998, and 2010. The negative IOD composite has been multiplied by -1 to ease comparison with the positive one.

Biogeosciences Discuss., doi:10.5194/bg-2016-195, 2016
Manuscript under review for journal Biogeosciences
Published: 9 June 2016

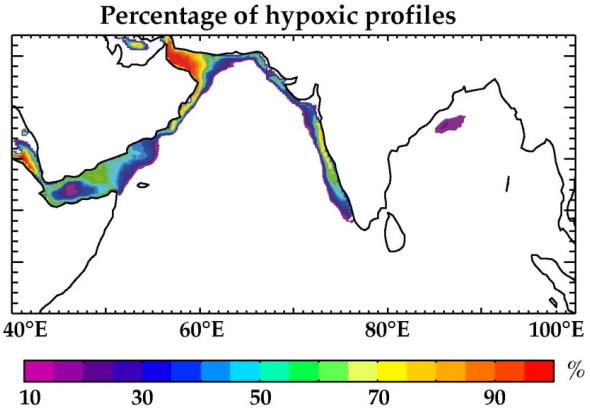

Figure 13. Percentage of occurrence of near-surface hypoxic conditions in the model during fall. Near-surface hypoxic conditions are defined as profiles with oxygen concentration below 80 μmol.l^{-1} (a threshold under which a most large marine organism suffer from stress) in the upper 50 m.